Materials Research Bulletin 51 (2014) 418–425

Contents lists available at ScienceDirect

Materials Research Bulletin

journal homepage: www.elsevier.com/locate/matresbu

$Lu_2O_3:Eu^{3+}$ glass ceramic films: Synthesis, structural and spectroscopic studies

M.L. Carrera Jota [a], A. García Murillo [b,*], F. Carrillo Romo [b], M. García Hernández [c], A. de J. Morales Ramírez [b], S. Velumani [d], E. de la Rosa Cruz [e], Abdelhadi Kassiba [f]

[a] Alumna del posgrado en Tecnología Avanzada del IPN CIITEC Azcapotzalco, Mexico
[b] Instituto Politécnico Nacional – CIITEC Azcapotzalco, Cerrada de Cecati S/N, Col. Santa Catarina, Del. Azcapotzalco, C.P. 02250 México, D.F., Mexico
[c] Departamento de Ciencias Naturales, DCNI, UAM Cuajimalpa, Pedro Antonio de los Santos 84, C.P. 11850 México, D.F., Mexico
[d] Instituto Politécnico Nacional, Centro de Investigación y de Estudios Avanzados (CINVESTAV), Departamento de Ingeniería Eléctrica (SEES), Av. Instituto Politécnico Nacional 2508, Col. San Pedro Zacatenco, C.P. 07360 México, D.F. Apartado Postal 14-740, 07000 México, D.F., Mexico
[e] Centro de Investigaciones en Óptica A.C., A.P. 1-94837150, León, Gto., Mexico
[f] Institut des Molécules et Matériaux du Mans, CNRS6283, Université du Maine, 72085 Le Mans Cedex 9, France

ARTICLE INFO

Article history:
Received 4 June 2013
Received in revised form 26 August 2013
Accepted 13 December 2013
Available online 19 December 2013

Keywords:
A. Optical materials
B. Sol–gel chemistry
C. Electron microscopy
C. X-ray diffraction
D. Luminescence

ABSTRACT

For the first time, transparent and crack free europium-doped lutetia silica sol–gel films were synthesized using the dip-coating technique on silica quartz substrates. In this study, we examined the effects of incorporating polyvinylpyrrolidone (PVP) and silica (SiO_2) into different precursor solutions for different Lu–Si molar ratios: 4:1, 6:1, 8:1 and 10:1. Different systems, such as $Lu_2O_3:Eu^{3+}@SiO_2$ (using the above Lu:Si molar ratios), were synthesized by sol–gel and by dip-coating technique, employing acetylacetonate lutetium and tetraethylorthosilicate as Lu and Si precursors, in order to produce $Lu_2O_3:Eu^{3+}$ (5 mol%)@SiO_2 glass–ceramic films. The film microstructure was studied by microRaman spectroscopy (MRS) and X-ray diffraction (XRD) for different Lu:Si molar ratios on films annealed at 700 °C. X-ray diffraction results showed that the lutetium oxide cubic phase crystallizes in the silica matrix at 700 °C, and the crystallite size of $Lu_2O_3:Eu^{3+}@SiO_2$ films varies from 5 nm to 17 nm according to the respective Lu:Si molar ratios. Opto-geometrical parameters determined by *m*-lines spectroscopy using a 632.5 nm He–Ne laser showed that the Eu^{3+} doped films heat-treated at 700 °C presented a thickness and density of 1.7 μm (8.8 g cm^{-3}), 970 nm (9.2 g cm^{-3}), 1 μm (9.3 g cm^{-3}) and 1.3 μm (9.25 g cm^{-3}) for the Lu:Si = 4:1, 6:1, 8:1 and 10:1 molar ratio systems, respectively. The Lu:Si = 8:1 system 611 nm emission presented an improvement. These results were provided by photoluminescent spectroscopy.

1. Introduction

Recently, there has been a growth of interest in the preparation of luminophores for developing research in medical areas such as X-ray imaging [1,2]. Such materials are often based on rare active crystals or ceramics due to their low cost, high concentration, and good dispersion of rare earth doping ions [3] compared with single crystal methods widely used at present. Europium activated dense Lu_2O_3 oxide powders are the most promising for X-ray detection and imaging because the exceptionally high density (~9.42 g cm^{-3}) and highly effective atomic number $Z_{eff.} = 67.3$ [4,5]. Due to its promising and well-known red emission, several studies have been devoted to studying ceramic light-emitting europium activated lutetium-based glass ceramic phosphors [6,7], especially because such ceramics are characterized by pronounced optical properties [8]. Thus, the SiO_2 core can provide the desired particle morphology, and the shell is responsible for the scintillation response formation of core–shell phosphors. However, preparation of Lu_2O_3 spherical particles with a narrow size distribution by conventional soft chemistry methods presents some difficulties.

In order to prepare the ultrafine, monosized, low-agglomerated and spherical powders, novel sol–gel strategies have resulted in significant simplification of procedures yielding transparent polycrystalline silica glasses activated with nanocrystallites [9,7]. Recently, some core–shell structured phosphors (SiO_2/$Y_2O_3:Eu^{3+}$ [10], $SiO_2/Gd_2O_3:Eu^{3+}$ [11], $SiO_2/YVO_4:Eu^{3+}$ [12], SiO_2/$GdVO_4:Eu^{3+}$ [13], $SiO_2@(Er^{3+},Yb^{3+}):Lu_2O_3$ [14], etc.) have been obtained and their preliminarily luminescent properties studied [15]. However there are no reports on the preparation and luminescence properties of europium doped lutetium oxide glass ceramic phosphor films. In this paper we report the elaboration,

* Corresponding author. Tel.: +52 55 5729 6000x68316; fax: +52 5561 7536.
E-mail address: angarciam@ipn.mx (A. García Murillo).

0025-5408/$ – see front matter © 2014 Published by Elsevier Ltd.
http://dx.doi.org/10.1016/j.materresbull.2013.12.029

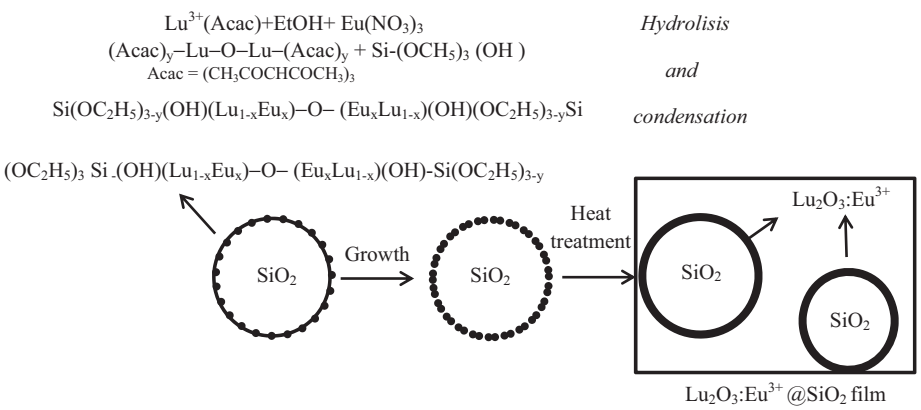

Scheme 1.

and the structural and photoluminescence properties of Eu^{3+} doped nanocrystallites embedded in silica glass ceramic films. In this manuscript, a thin film of $Lu_2O_3:Eu^{3+}$ was formed on the surface of nanometer spherical silica by using a sol–gel method, leading the formation of $Lu_2O_3:Eu^{3+}@SiO_2$ core–shell submicrospheres well distributed in SiO_2 films (Scheme 1).

The main objective of this study is to establish the synthesis procedure and the structural evolution of europium doped Lu_2O_3 photoluminescent glass ceramic sol–gel films as a function of different Lu:Si molar ratios using X-ray diffraction (XRD) and microRaman spectroscopy techniques. Scanning electron microscopy (SEM) was utilized on $Lu_2O_3:Eu^{3+}@SiO_2$ films to confirm Raman observations. The spectroscopic properties make $Lu_2O_3:Eu^{3+}@SiO_2$ prepared in the described way a promising X-ray phosphor for planar digital X-ray medical imaging systems.

2. Experimental

2.1. Preparation of 5 mol% Eu^{3+} doped Lu_2O_3 glass ceramic films

Europium doped Lu_2O_3 glass ceramic films obtained by sol–gel process were prepared using two precursor solutions: $Lu_2O_3:Eu^{3+}$ and SiO_2 sols. Details of the $Lu_2O_3:Eu^{3+}$ and SiO_2 synthesis procedures are described elsewhere [16,17]. A yellow and transparent sol was prepared by dissolving the lutetium(III)-2,4-pentanedionate $Lu(CH_3COCHCOCH_3)_3$ precursor in anhydrous isopropanol and thereafter the europium(III) nitrate pentahydrate $Eu(NO_3)_3{\cdot}5H_2O$ 99.9% is added in order to obtain the 5 mol% Eu^{3+} stable precursor "sol". This feature is a characteristic important to ensuring reproducible coatings in order to prepare multicoated films. The raw materials for SiO_2 synthesis were: tetraethylorthosilicate TEOS ($Si(OC_2H_5)_4$, ≥99.0%, Fluka), ethylic alcohol (C_2H_6O, Fermont, 99.9%), distilled water and chloride acid (HCl) (37% Fermont) as a catalyst. The molar ratio of ethylic alcohol/TEOS and TEOS/water was kept at 4:1 and 6:1, respectively. Distilled water and HCl were added in appropriate quantities to the solution in order to adjust the pH to 4. The preparation of Lu_2O_3 glass ceramics by sol–gel process was executed by mixing $Lu_2O_3:Eu^{3+}$ sol into SiO_2 sol in molar ratios of Lu:Si 4:1, 6:1, 8:1 and 10:1 (Fig. 1). Finally, polyvinylpyrrolidone (PVP) was slowly incorporated into the sol, with a PVP/Lu molar ratio of 0.75:1 (PVP molecular weight = 1,300,000). $Lu_2O_3:Eu^{3+}$ material was also prepared for reference. The europium doped lutetium silica precursor solution filtered through 0.22 μm was dip-coated on silica quartz substrates. The solutions were dip-coated on highly polished and carefully cleaned silica substrates (Herasil from Heraeus®), with a constant withdrawal speed of 12 cm s^{-1} in a glove box to avoid dust contamination. Two and five layers were deposited and heat treated at 300 °C for 10 min between each coating. At the end, the formed films were heat treated at different temperatures ranging from 300 °C to 700 °C. At this stage, crack free and transparent europium doped lutetium oxide glass ceramic multilayers were obtained.

2.2. Apparatus

Raman spectroscopy was conducted on the europium doped lutetia glass ceramic films and also on the cubic reference powder. The microRaman spectra were carried out using a Horiba-Jobin Yvon micro Raman apparatus (LabRAM HR800). The microRaman

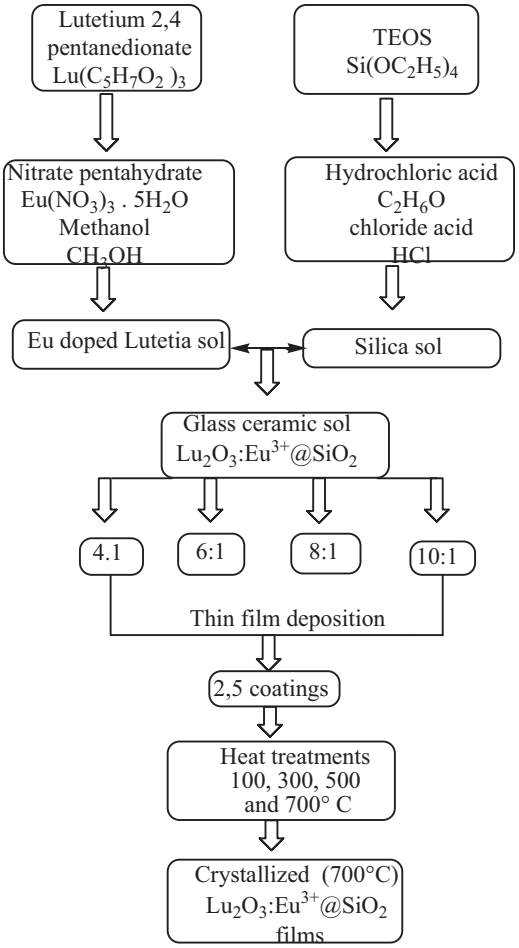

Fig. 1. Synthesis procedure of $Lu_2O_3:Eu^{3+}@SiO_2$ films.

spectra were recorded in the range 150–1000 cm^{-1} using a He–Ne beam (λ = 632.61 nm). The crystal structure of the doped glass ceramic films was determined by X-ray diffraction (XRD) technique by an automated powder diffractometer (Siemens D5000). Cu Kα monochromatized radiation operated at the following setting: 35 kV, 25 mA, with a graphite monochromator selecting Cu Kα radiation (λ = 1.54056 Å). A step of 0.15°/s was used in the 15–90° (2θ) angular domains, using grazing angle configuration. The crystallite size D (nm) in films, calculated from the width of the main diffraction peak line (2 2 2), was estimated by the Debye–Scherer equation: $D = 0.9\lambda/\beta \cos\theta$, where λ (nm) represents the wavelength of the Cu Kα radiation (1.54056 Å), θ is the Braggs's angle and β represents the full width at half maximum (FWHM) of the main peak, where $\beta = (\beta^2_{meas} - \beta^2_{equip})^{1/2}$, β_{meas} = measured FWHM and β_{equip} = FWHM due to instrumental broadening. The microstructure of glass ceramic films was determined by using a scanning electron microscope (JEOL JSM-6390LV). The AFM analyses were performed in air and at room temperature on a microscope (Nanosurf Easyscan2) in tapping mode using a tip made of antimony-doped Si with an aluminum reflective coating on the backside. The scan rate was about 1 Hz. For each sample, at least four areas were imaged in height and phase mode. *M*-lines spectroscopy is a useful method to determine the optogeometric parameters of thin films [18], such as thickness and refractive index; n_{TE} and n_{TM} in both transverse magnetic (TM) and/or transverse electric (TE) polarizations using He–Ne laser with λ = 632.8 nm. PL characterization was performed with a 75 W white light source (xenon lamp). The fluorescence emission was analyzed with an Acton Research modular 2300 spectrofluorometer and a R955 Hamamatsu photomultiplier tube for visible emission. The emission spectra were measured and analyzed by using excitation at 252 nm. The system was PC controlled with Spectra-Sense software. Special care was taken to maintain the alignment of the setup in order to compare the intensities between different characterized samples. Fluorescence decay time was measured using an SR540 chopper from Stanford, Inc., the monochromator and the photomultiplier connected to a Tektronix TDS3052B digital oscilloscope. All the experiments were performed at room temperature.

3. Results and discussion

3.1. Phase identification and structural properties

In order to study the structural characteristics of europium doped lutetium oxide glass ceramic films deposited on silica substrates, X-ray diffraction patterns were recorded on different Lu:Si molar ratios Lu_2O_3:Eu^{3+}@SiO_2 films heat treated at 500, 600 and 700 °C for 10 min (Fig. 2). The crystallization of the powder occurs at up to 500 °C and 600 °C (not shown here). As annealing temperature increased up to 700 °C, the diffraction lines became sharp; the diffraction peaks around 2θ = 29.6° (2 2 2), 34.2° (4 0 0), 49.5° (4 4 0) and 58.5° (6 2 2) matched perfectly with the cubic C-Lu_2O_3 (JCPDS 43-1021) structure of the reference ceramic film [19]. The C-Lu_2O_3 phase has been extensively investigated to form promising photoluminescent properties of rare-earth doped Lu_2O_3 systems [4,5]. The broad band peaking at 2θ = 21° is characteristic of amorphous silica. The absence of crystalline peaks superimposed on the amorphous band in the 2θ = 25–33° range suggests a complete crystallization of Lu_2O_3:Eu^{3+} into an SiO_2 amorphous matrix after 700 °C thermal treatment. The crystallite size of the Lu_2O_3:Eu^{3+}@SiO_2 films were 17, 10, 5 and 7 nm for Lu_2O_3:Eu^{3+} (Lu:Si 4:1, 6:1, 8:1 and 10:1 glass ceramic films, respectively), and for the Lu_2O_3:Eu^{3+} films the size was 21 nm.

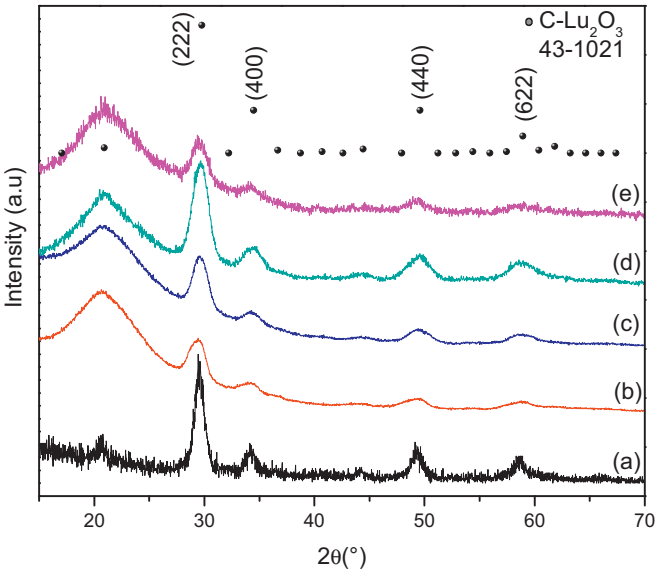

Fig. 2. XRD patterns of Lu_2O_3:Eu^{3+} films heat-treated at 700 °C at different Lu:Si molar ratios, 100:0 (a), 4:1 (b), 6:1 (c), 8:1 (d) and 10:1 (e).

3.1.1. Raman studies

In order to study the structural characteristics of europium doped lutetium oxide films, Raman analyses were conducted on Lu_2O_3:Eu^{3+} glass ceramic films.

Fig. 3 shows the Raman spectra of Lu_2O_3:Eu^{3+} glass ceramic films and also the Lu_2O_3:Eu^{3+} film. The Raman bands observed on lutetium oxide glass ceramic films heat treated at 700 °C are consistent with the characteristic spectrum of europium doped Lu_2O_3 film thermally treated at the same temperature. The main bands appears around 390 cm^{-1}, 120 cm^{-1}, 146 cm^{-1}, 348 cm^{-1}, 454 cm^{-1}, 499 cm^{-1} and 611 cm^{-1}, as reported in a previous study [19], the most characteristic band being the one at 390 cm^{-1}. In all the glass ceramic systems, the band at 390 cm^{-1}, associated with C-Lu_2O_3, is present. In addition to those bands, the 4 samples of Lu:Si in different molar ratios exhibited Raman bands associated with silica bands observed at 490 cm^{-1} (D1) and 610 cm^{-1} (D2) which are attributed to the symmetric stretching modes of vibrationally isolated rings of SiO_2 tetrahedra [20]. In addition to the normal silica bands, bands also peaked at 440 cm^{-1} and 1060 cm^{-1}, which is attributed to the ν_1 bending and ν_4 transversal optic modes of oxygen atoms in siloxane bond Si–O–Si.

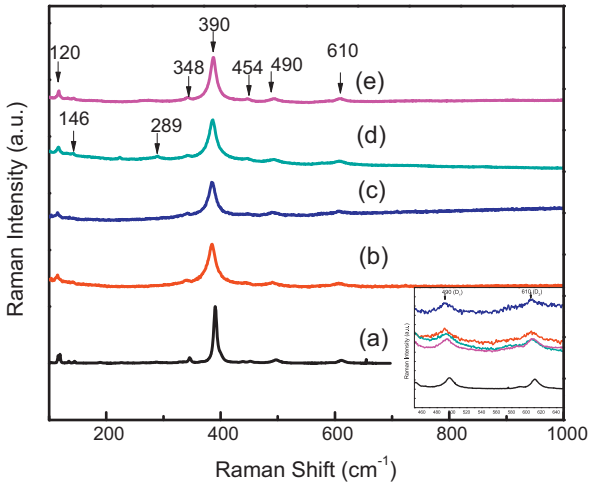

Fig. 3. MicroRaman spectra of Lu_2O_3:Eu^{3+}@SiO_2 films at different Lu:Si molar ratios: 4:1 (a), 6:1 (b), 8:1 (c) and 10:1 (d).

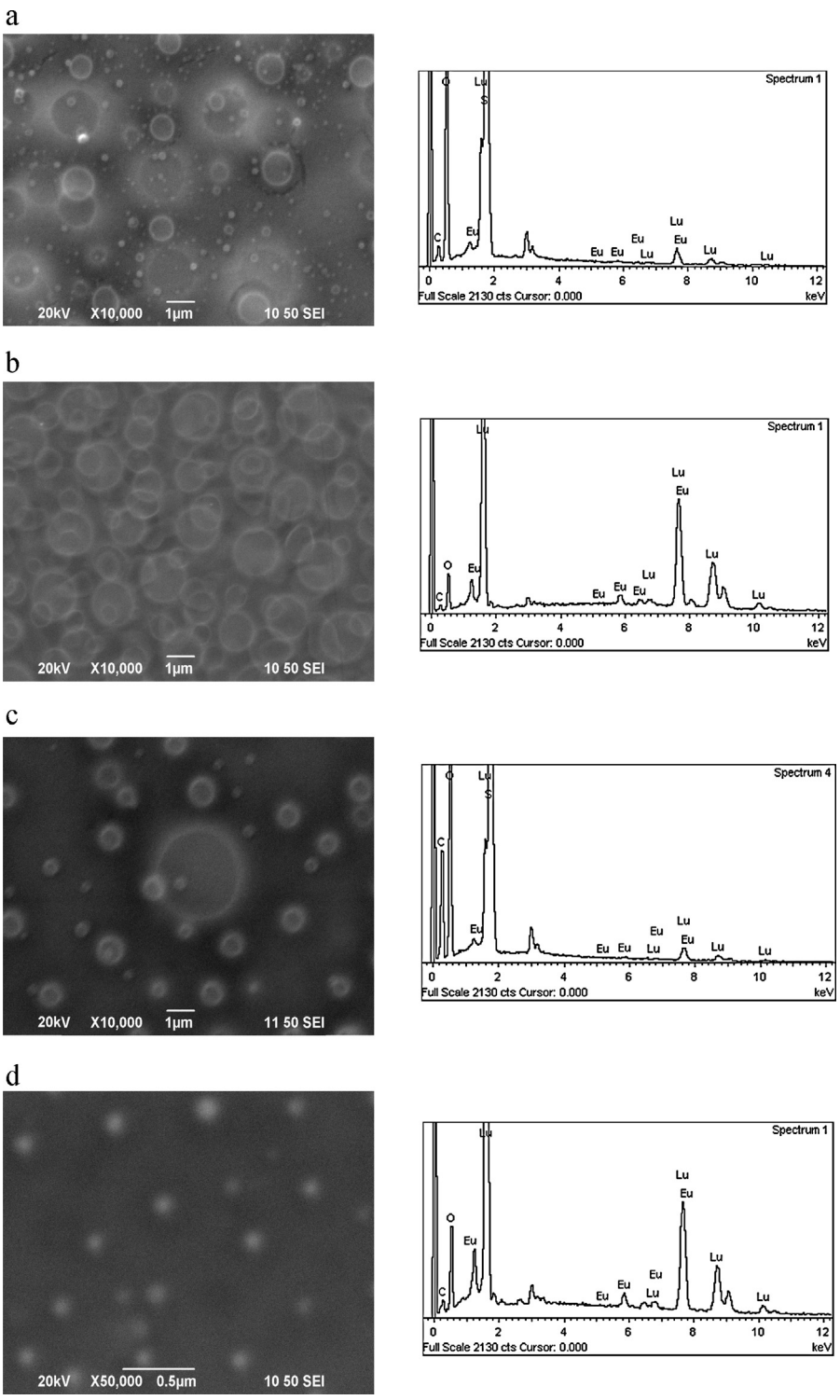

Fig. 4. SEM images of $Lu_2O_3:Eu^{3+}@SiO_2$ films heat treated at 700 °C for different Lu:Si molar ratios 4:1 (a), 6:1 (b), 8:1 (c) and 10:1 (d).

3.2. Microstructural properties of $Lu_2O_3:Eu^{3+}$ films

3.2.1. Morphological studies (SEM)

The morphological study was conducted on the lutetium oxide films using a scanning electron microscope (SEM) with a field emission gun. The surface morphology of the $Lu_2O_3:Eu^{3+}$ glass ceramic films obtained at different Lu:Si molar ratios is presented in Fig. 4a–d. This structure was carefully analyzed, taking into account the optical feature of the layers that present waveguide properties. The microstructure of the $Lu_2O_3:Eu^{3+}@SiO_2$ in presence of PVP and heat treated at 700 °C analyzed on a large scale reveals the presence of freshly prepared spheres for different Lu:Si molar ratios. For example, the films with Lu:Si = 4:1 and 6:1 (Fig. 4a and b) reveal the presence of particles with a perfect spherical shape and uniform size distribution characterized by a mean diameter ranging between 63 and 627 and 580 nm, respectively. For these Lu:Si systems it was observed a decrease in mean diameter from 627 nm (Fig. 4a) in the Lu:Si = 4:1 film to 63 nm (Fig. 4d) corresponding to Lu:Si = 10:1. The Lu:Si = 8:1 film (Fig. 4c) particles have uniform mean sizes of 440 nm and are not

agglomerated. The image for the Lu:Si = 10:1 film (Fig. 4d) shows smaller (around 63 nm) and well-distributed spherical particles. In all the Lu_2O_3:Eu@SiO_2 systems this feature is present, which is related with the presence of a PVP capping agent. The molecular weight of this agent is an important aspect, but also the molar concentration used. For example, with a 1.3 million molecular weight of PVP a formation of decahedron nanostructure occurs [21]. Nevertheless some studies report that an equivalent concentration of PVP with some metal salts precursors will result in predominantly spherical nanoparticles [22]. This means that PVP coordinates with metal ions through C–N and C=O bonds, stabilizing the nanoparticles contained in the precursor solution [23]. The present Lu_2O_3:Eu^{3+}@SiO_2 films prepared from PVP-containing stable sols, which led to the formation of transparent and homogeneous structures promoted by an initial stage consisting of phase separation between polymeric species and solvents. The addition of SiO_2 into the precursor solution reduces surface tension, thus favoring the formation of spheres. The formation of crack-free films is due to the thermal treatment performed.

The successive coatings were prepared at a temperature lower than 350 °C. When the crack formation occurred, the films were directly heat-treated at 500 °C, allowing the decomposition of PVP and CH_3COO^- and favoring the formation of lutetium oxide. This heat-treatment condition provides an effective process to produce dense, well crystallized and optical quality films.

The energy dispersive X-ray spectrum (EDS) of precursor particles shows the peaks which are attributed to Lu, O and C elements (Fig. 4b). According to the EDS results, the Eu doping level is about 5.5 ± 0.4% mol, (analyzing 5 different micrographs). Also, the stoichiometry of the Si–O compound is about SiO_x (x = 1.8 ± 0.2).

3.2.2. Atomic force microscopy characterization

In order to study the surface morphology, atomic force microscopy was conducted on the Lu_2O_3:Eu^{3+}@SiO_2 films. Top-view and three-dimensional images of the different Lu:Si molar ratios films annealed at 700 °C are shown in Fig. 5. The morphology of the film composed by Lu:Si = 4:1 molar ratio (Fig. 5a) exhibited a homogeneous surface for all systems: Lu:Si = 4:1, 6:1 (Fig. 5b), 8:1 (Fig. 5c) and 10:1 (Fig. 5d), and a well-crystallized morphology with a small RMS roughness of 8, 13.4, 4.7 and 4.8 nm (Fig. 5a–d), respectively. It can be seen from Fig. 5a that the Lu_2O_3 crystallites are uniform with a spheroidal shape. The average size of the crystallite is estimated to be around 5–17 nm, which is consistent with the XRD results by Scherrer's equation. The films calcined at 700 °C are uniform and crack free, consisting of closely packed particles with an average size of about 48–627 nm.

3.3. M-lines spectroscopy

This technique was used on the multilayer films. Two transverse electric (TE) and two transverse magnetic (TM) modes were observed in samples heat-treated at 300–700 °C for 10 min.

Films with 5 stacked layers can support two TE modes and two TM modes (TE_0, TE_1, TM_0, TM_1, respectively). These propagation modes, of the same polarization, are the minimum requirement for calculation of optogeometrical parameters [24]. The refractive indices and thickness of cubic Lu_2O_3:Eu^{3+} glass ceramic films at different Lu:Si molar ratios in TE polarization, and heat treated at 700 °C, are presented in Fig. 6. Results (Fig. 6) measured at 632.8 nm show that the film thickness is a function of the Lu:Si molar ratios corresponding to those presented in Table 1. The determined refractive indices for the studied films could be related to Lu:Si content; for example, in the cases of the Lu:Si systems 4:1 and 10:1, the 4:1 molar ratio presents the highest Si content which diminishes the refractive value. The lowest refractive index

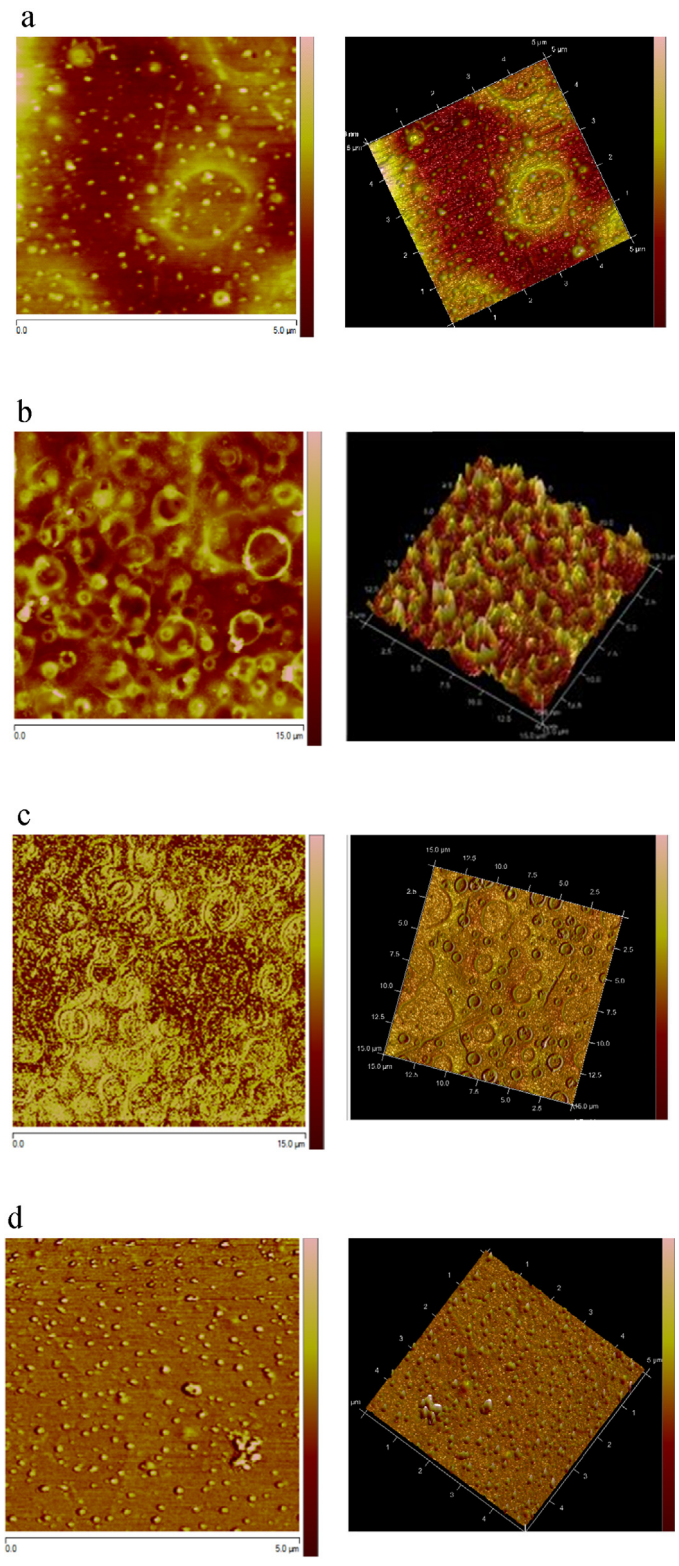

Fig. 5. Top-view AFM topography micrographs of Lu_2O_3:Eu^{3+}@SiO_2 films heat treated at 700 °C for different Lu:Si molar ratios 4:1 (a), 6:1 (b), 8:1 (c) and 10:1 (d).

corresponds with the highest obtained thickness. The contrary is true for the 10:1 molar ratio: the Si content is the lowest and the film reveals the highest refractive index value and the lowest thickness, being a film with a behavior closer to Lu_2O_3:Eu^{3+} films (Fig. 6). For the intermediate molar ratios 6:1 and 8:1, these optogeometrical characteristics consist in n and e values governed (probably) by better the crystallization and densification process

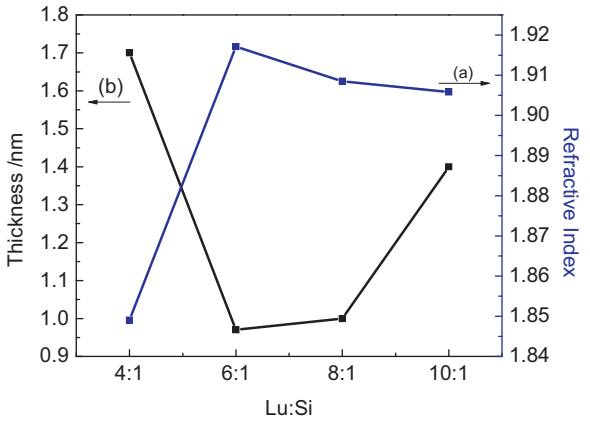

Fig. 6. Evolution of refractive index at 632.8 nm (a) and thickness (b) of Lu_2O_3@SiO_2 for different Lu:Si molar ratios.

attributed predominantly to Lu_2O_3:Eu^{3+} formation. The film thickness is favored by the high Si content, thereby the film with a 4:1 molar ratio yields a convenient Lu:Si molar ratio characterized by a well-densified Lu_2O_3:Eu^{3+} ceramic.

From the simplified Lorenz–Lorentz equation [20] $d_{film} = K((n^2_{film(\lambda)} - 1)/(n^2_{film(\lambda)} + 2))$ using the refractive index on TE modes at 632.8 nm and also the Drude equation [21] $1 - p = (n_f^2 - 1)/(n_b^2 - 1)$; it is possible to evaluate the density and deduce a mean value of the film porosity p. In the equation, p is porosity, and the bulk Lu_2O_3 refractive index n_b and our Lu:Si = 8:1 glass ceramic films n_f are 1.92 and 1.908, respectively. So the porosity of the Lu_2O_3:Eu^{3+} glass ceramic films (Table 2) is lower than 11%, which are lower values in comparison with that of dense Lu_2O_3 [16] films (calculated porosity around 19%).

3.4. Luminescent properties of Lu_2O_3:Eu^{3+}@SiO_2 layers

Fig. 7 shows the excitation (λ_{em} = 611 nm) and emission (λ_{ex} = 252 nm) spectra of Lu_2O_3:Eu^{3+} films and Lu_2O_3:Eu@SiO_2 glass ceramic films, respectively, all of them recorded at room temperature.

The excitation spectrum reveals a wide band with a maximum at 252 nm, which is attributed to the O^{2-}–Eu^{3+} charge transfer band (CTB). Additionally, a very weak band arising from 4f transitions appears. The excitation spectra indicate that the host material is able to transfer acquired energy to the Eu^{3+} ions and cause the characteristic red emission of Eu^{3+} in Lu_2O_3:Eu@SiO_2 glass ceramic films. The photoluminescence emission spectra of Lu_2O_3:Eu^{3+}@SiO_2 glass ceramic films, and also that of Lu_2O_3:Eu^{3+} film for comparison, consist of the interconfigurational $^5D_0 \rightarrow {}^7F_J$ (J = 0–3) transition of Eu^{3+}, dominated by the $^5D_0 \rightarrow {}^7F_2$ (611 nm). Nevertheless, there are some differences for different Si content. It can be seen that the silica host weakly affects the structure of the surroundings of Eu^{3+}emitted ions. The broadening of emission peaks with the increase of Si content can be observed in the emission spectra. The photoluminescence could be affected by the uniform size, non agglomeration and shape of particles

Table 1
Optogeometrical parameters of Lu_2O_3:Eu^{3+}@SiO_2 films heat treated at 700 °C for different Lu:Si molar ratios 4:1 (a), 6:1 (b), 8:1 (c) and 10:1 (d).

Lu:Si molar ratios	Refractive index	Thickness (μm)
4:1	1.849 ± 0.001	1.7
6:1	1.917 ± 0.001	0.97
8:1	1.908 ± 0.001	1.0
10:1	1.905 ± 0.001	1.4

Table 2
Physical characteristics of Lu_2O_3:Eu^{3+}@SiO_2 films heat treated at 700 °C for different Lu:Si molar ratios 4:1 (a), 6:1 (b), 8:1 (c) and 10:1 (d).

dm = 9.4 g cm^{-3} nm = 1.92	T (°C)	Porosity (%)	Density (g cm^{-3})
4:1	700	11	8.8
6:1	700	3	9.25
8:1	700	2	9.3
10:1	700	3	9.25

characterizing the different Lu:Si molar ratio films. First of all, the relative intensity of f–f transition increases greatly compared to powder materials. Second, as the Si content decreases, the particle size increases from 63 nm to 627 nm for Lu:Si 10:1 to reach a 4:1 molar ratio. Third, as the Lu_2O_3:Eu^{3+} particles are embedded in a more and more reduced SiO_2 content, the photoluminescence emission increased up to that of a Lu:Si = 8:1 molar ratio system. Subsequently, as the Lu:Si content lowers, a luminescence quenching is observed In this case, we suppose that the critical Si content is responsible for this phenomenon. The Eu^{3+} ions in a low SiO_2 content (fine SiO_2 layer) experience a different ligand environment and distinct crystal fields compared to that observed for higher Si contents. The energy levels of Eu^{3+} are slightly different from those of composite particles (Lu:Si = 10:1) ~63 nm (monomodal distribution) in size compared to bigger and less distributed particles; i.e. the Lu:Si = 8:1 system leads Lu_2O_3:Eu^{3+}@-SiO_2 to disperse particles in a homogeneous film, in contrast with that of Lu:Si = 10:1 systems, which leads to the slight broadening of spectra [25]. The particle size increases with the SiO_2 molar content, which results in a different crystallinity, influencing their spectroscopic properties [28]. Fig. 8a shows the luminescence intensity of Lu_2O_3:Eu^{3+} (5 mol%)@SiO_2 films depending on particle size and SiO_2 molar content. It is clearly seen that with the increasing of the SiO_2 content up to Lu:Si = 8:1, the luminescence intensity increases. This fact could be related to the improvement of the particles' crystallinity, as the SiO_2 content diminishes on the Lu_2O_3:Eu^{3+} glass ceramic films. As the Lu:Si molar ratio is bigger than 8:1, the lower coating particles' atom-volume percentage of interface increases, and defects of the surface also increase, which results in the increase of the surface-to-volume ratio and the content of defects and/or impurities in the particle, making the bond length of the surface and interior different. The bond length of the interface has a broader distribution; thus the energy is not uniform and the energy level broadens, so the emitting peaks are thus broadened [11]. The high excitation efficiency of the luminescence impurity of Lu_2O_3:Eu^{3+} films is a consequence of efficient energy transfer processes forming the lattice to luminescence centers (europium ions) via a hole recombination mechanism [26]. Lu_2O_3:Eu^{3+}@SiO_2 in the nanocrystalline form is known as a material that exhibits multiplication of electronic excitations. The photonic multiplications start at the energies of 2–4 Eg due to generation of secondary electron–hole pairs by hot carriers, leading to the increase of the luminescence yield of Eu^{3+} centers [27]. The multiplication of electronic excitation in Lu_2O_3:Eu^{3+} nanocrystals in the $h\nu > 14$ eV energy range is one of the reasons for their use as effective scintillators with quantum yields higher than 1. The fluorescence decay curves for the $^5D_0 \rightarrow {}^7F_2$ transition (612 nm) of Eu^{3+} in Lu_2O_3:Eu^{3+}@SiO_2 glass ceramic films for different Lu:Si molar ratios were recorded at room temperature. The recorded decay curves were mathematically derived time constants for Lu_2O_3:Eu^{3+}@SiO_2 films (presented in Fig. 8b). In the case of the as-prepared films, the decay curves do not change significantly with the SiO_2 content. Similar lifetimes obtained for the Lu_2O_3:Eu^{3+} glass ceramic films were reported for Lu_2O_3:Eu^{3+} nanocrystallites [27]. The $^5D_0$ state can be populated by the two

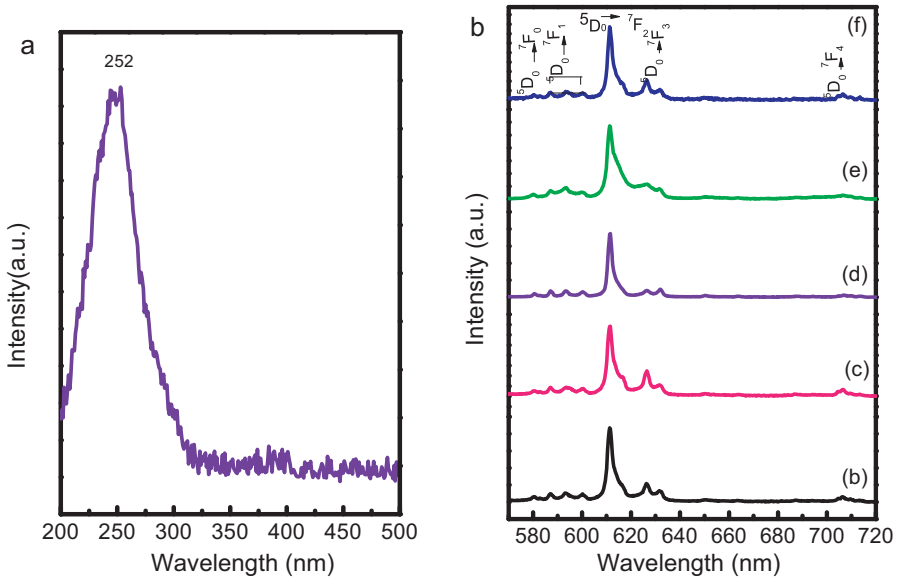

Fig. 7. Room temperature excitation (a) and emission spectra under 252 nm excitation of $Lu_2O_3:Eu^{3+}@SiO_2$ films heat treated at 700 °C for different Lu:Si molar ratios 4:1 (b), 6:1 (c), 8:1 (d) 10:1 (e) and $Lu_2O_3:Eu^{3+}$ film (f).

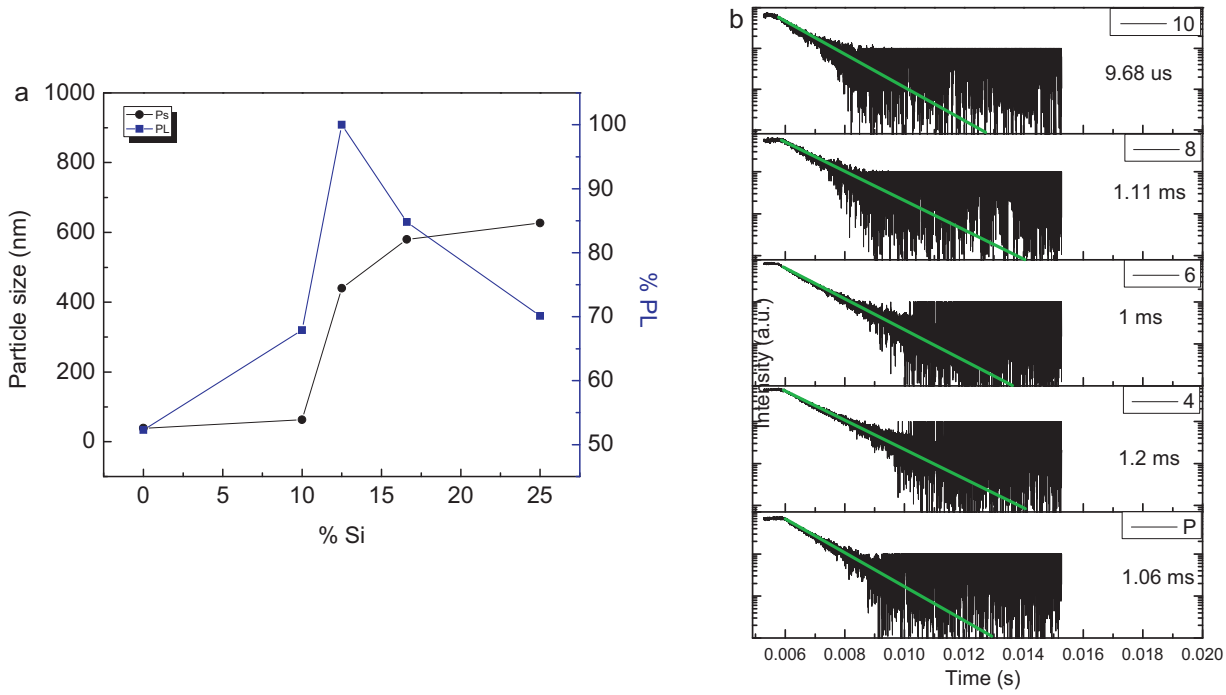

Fig. 8. Luminescence intensity dependence on particle size and SiO_2 content (a), and fluorescence decay curves of $Lu_2O_3:Eu^{3+}@SiO_2$ films for different Lu:Si molar ratios 4:1, 6:1, 8:1 and 10:1 (b).

processes, a non-radiative multi-phonon relaxation from the higher levels or a cross-relaxation [28]. All the decay curves rise first and then decay. The same appearance of the rise time, which indicates the presence of some slow relaxation processes feeding the emitting level ($^5D_0$), was observed by Guo et al. [29]. We did not observe significant differences in the emission decay times of $Lu_2O_3:Eu^{3+}$ glass ceramic films and those of $Lu_2O_3:Eu^{3+}$ ceramic films reported by García-Murillo et al. [30]. In this case, the as-prepared glass ceramic films do not exhibit the luminescence of Eu^{3+} quench produced by multiphonon relaxation; nevertheless some studies revealed that the luminescence of europium ions which have migrated to the crystallite surface will be quenched [31], which, in turn, will influence the decay times [32].

4. Conclusions

Non-agglomerated and well-dispersed spherical $Lu_2O_3:Eu^{3+}@SiO_2$ particles with sizes ranging from 63 to 627 nm constituting glass ceramic films were synthesized by sol–gel process after being heat-treated at 700 °C for 10 min. The films presented a perfect cubic structure. The presence of SiO_2 and PVP promotes the formation of thick low porosity (<11%) film between 1 and 1.7 μm depending on Lu:Si molar content. The refractive index (around 1.9) does not change for the Lu:Si molar ratios studied. The changes of emission spectra and fluorescence decay times of $Lu_2O_3:Eu^{3+}$ glass ceramic films show that the amount of silica spheres has an obvious influence on the luminescence properties of the

Lu_2O_3:Eu^{3+} shell. For the lifetimes observed around 1 ms, the sites of emitting Eu^{3+} ions of in the amorphous SiO_2 do change the environment similar to that in Lu_2O_3 ceramic films. For all the Lu:Si molar ratios, the, the decay curves of the glass ceramic films do not change significantly with the SiO_2 content. The technique presented here serves as a promising route toward the fabrication of low-cost and highly fluorescent glass ceramic phosphors, which may be convenient for scintillator applications.

Acknowledgements

The authors gratefully acknowledge the financial support of SEP-CONACYT (100764, 136269 and 178817) and SIP – IPN (20130665 and 20130664) projects. M.L. Carrera Jota acknowledges the M.Sc. scholarship from CONACYT. The authors thank the experimental support of CNMN-IPN for structural studies. The authors thank Eng. Alfonso R. for his help in SEM work and Haggeo S. for his technical support in luminescence studies. The authors also would like to thank David Nentwick for the editing work that he did for this paper. The authors would also like to thank M. García Murillo for her assistance.

References

[1] R. Morlotti, M.M. Nikl, M. Piazza, J. Lumin. 72–74 (1997) 772–774.
[2] I. Kandarakis, D. Cavouras, I. Sianoudis, D. Nikolopoulos, A. Episkopakis, D. Linardatos, D. Margetis, E. Nirgianaki, M. Roussou, P. Melissaropoulos, N. Kalivas, I. Kalatzis, K. Kourkoutas, N. Dimitropoulos, A. Louizi, C. Nomicos, G. Panayiotakis, Nucl. Instr. Meth. Phys. Res. A 538 (2005) 615–630.
[3] A. Lempicki, A.J. Wojtowics, C. Brecher, in: S.R. Rotman (Ed.), Wide-Gap Luminescent Materials: Theory and Applications, Kluwer, MA, 1996.
[4] X.-J. Liu, H.-L. Li, R.-J. Xie, N. Hirosaki, X. Xu, L.-P. Huang, J. Lumin. 127 (2) (2007) 469–473.
[5] C. Dujardin, A. García-Murillo, C. Pédrini, C. Madej, C. Goutaudier, A. Koch, A.G. Petrosyan, M.J. Weber, in: Proceedings of the Fifth International Conference on Inorganic Scintillators and Their Applications, 1999, pp. 527–531.
[6] E. Zych, J. Trojan-Piegza, J. Lumin. 122–123 (2007) 335–338.
[7] E. Zych, M. Wawrzyniak, A. Kossek, J. Trojan-Piegza, L. Kepinski, J. Alloys Compd. 451 (2008) 582–585.
[8] M. Daldosso, J. Sokolnicki, L. Kepinski, J. Legendziewicz, A. Speghini, M. Bettinelli, J. Lumin. 122–123 (2007) 858–861.
[9] E. Zych, J. Phys.: Condens. Matter 14 (2002) 5637–5650.
[10] H.-J. Feng, Y. Chen, F.-Q. Tang, J. Ren, Mater. Lett. 60 (2006) 737–740.
[11] G. Liu, G. Hong, D. Sun, J. Colloid Interface Sci. 278 (2004) 133–138.
[12] Y. Wangb, W. Qin, J. Zhang, C. Cao, S. Lü, X. Ren, Opt. Commun. 282 (2009) 1148–1153.
[13] G. Li, Z. Wang, M. Yu, Z. Quan, J. Lin, J. Solid State Chem. 179 (2006) 2698–2706.
[14] E. William Barrera, M. Cinta Pujol, C. Cascales, J.J. Carvajal, X. Mateos, R. Solé, Opt. Mater. 34 (2011) 355–359.
[15] Yu.V. Yermolayeva, T.I. Korshikova, A.V. Tolmachev, R.P. Yavetskiy, Radiat. Meas. 46 (2011) 551–554.
[16] A. García Murillo, F.d.J. Carrillo Romo, C. Le Luyer, A.d.J. Morales Ramírez, M. García Hernández, J. Moreno Palmerin, J. Sol–Gel Sci. Technol. 50 (2009) 359–367.
[17] F. Carrillo Romo, A. García Murillo, D. López Torres, N. Cayetano Castro, V.H. Romero, E. de la Rosa, V. Garibay Febles, M. García Hernández, Opt. Mater. 32 (2010) 1471–1479.
[18] M. Ulrich, R. Torge, Appl. Opt. 12 (1973) 2901.
[19] A. García-Murillo, C. Le Luyer, C. Pédrini, J. Mugnier, J. Alloys Compd. 323–324 (2001) 74–75.
[20] F.L. Galeener, Phys. Rev. B 19 (1979) 4292.
[21] Y. Gao, P. Jiang, L. Song, J.X. Wang, L.F. Liu, D.F. Liu, et al. J. Cryst. Growth 289 (2006) 376–380.
[22] I. Pastoriza-Santos, L.M. Liz-Marzan, Langmuir 18 (2002) 2888–2894.
[23] V. Sáez, T.J. Mason, Molecules 14 (10) (2009) 4284–4299.
[24] C. Urlacher, J. Mugnier, J. Raman Spectrosc. 27 (1996) 785.
[25] G. Blasse, B.C. Grabmaier, Luminescent Materials, Springer-Verlag, Berlin, 1994.
[26] V.N. Makhov, Ch. Lushchik, A. Lushchik, et al. J. Lumin. 129 (2009) 1711.
[27] D. Hreniak, et al. J. Phys. Chem. Solids 64 (2003) 111–119.
[28] J. Trojan-Piegza, E. Zych, D. Hreniak, W. Stręk, L. Kepinski, J. Phys.: Condens. Matter 16 (2004) 6983.
[29] H. Guo, et al. Appl. Surf. Sci. 243 (2005) 243–250.
[30] A. García-Murillo, C. Le Luyer, C. Dujardin, T. Martin, C. Garapon, C. Pédrini, J. Mugnier, Nucl. Instr. Meth. Phys. Res. A 486 (2002) 181–185.
[31] N.V. Babayevsakaya, et al. Funct. Mater. 17 (4) (2010).
[32] Z. Wang, et al. Opt. Mater. 30 (2008) 1484–1488.